Proceedings of the 22nd International Conference on
Port and Ocean Engineering under Arctic Conditions
June 9-13, 2013
Espoo, Finland

LABORATORY STUDIES OF OIL ENCAPSULATION UNDER GROWING SEA ICE

Chris Petrich and Martin Arntsen

Norut Narvik AS, 8504 Narvik, Norway

ABSTRACT

Oil reaching the underside of sea ice after a blow-out is able to spread laterally, governed by buoyancy and surface tension, under-ice topography, and currents. However, the possibility of lateral spread and the direct contact with the ocean are inhibited once oil begins to get encapsulated by the advancing ice front. Encapsulation removes oil largely from the environment, influencing risk management strategies. We performed laboratory tank experiments to quantify the encapsulation process. A 130 L tank was built from Perspex with removable insulation to allow for in-situ observation of the ice underside. Heat flux into the water was controlled to ensure the development of a realistic crystal fabric. Oil was injected under ice of 0.1 m thickness. Observations on crystal structure and encapsulation process are consistent with previous studies. Following the initial development of a lip around the oil lens, initial overgrowth was due to crystals with vertical c-axes. Temperature probes recorded vertical heat flux and ice growth rate under the lens. Encapsulation appeared to be governed by common thermodynamic and fluid dynamic principles. No indications were found that crystal alignment would need to be considered explicitly to describe encapsulation numerically.

INTRODUCTION

Oil spilled under sea ice during the ice growth season impinges on the ice underside and spreads laterally in response to buoyancy, the ice bottom profile, surface tension, and ocean currents. Once the oil comes to a rest, sea ice growth continues around it, encapsulating the oil lens, and allowing oil to entrain the ice above (e.g., Karlsson et al., 2011; Petrich et al., 2013). While a number of oil spill experiments have been performed under Arctic sea ice (e.g., Dickins, 2011), laboratory experiments have been used to study the encapsulation process in more detail (e.g., Wolfe & Hoult, 1974; Payne et al., 1991; Dickins, 1992).

We performed a range of laboratory experiments in which oil was injected under a sea ice cover. Ice growth process was monitored visually and with thermocouple probes, and ice structure and properties were analysed after excavation of ice.

In the absence of a model of oil lens encapsulation (Dickins, 1992), this work was aimed to illuminate the process of encapsulation in search of processes that were incompatible with thermodynamic considerations.

METHODS

Ice was grown in a Perspex tank with 5 mm thick walls. The tank was 0.5 m high, and had a cross sectional area of 0.5 x 0.5 m^2 and 0.5 x 0.52 m^2 at the bottom and top, respectively (Figure 1a). The tank was insulated with removable 0.05 m-thick foam plates (manufacturer-supplied thermal conductivity k=0.036 W $m^{-1}K^{-1}$). A 0.05 m air gap under the tank housed resistors and a fan for heating, digital cameras to record ice growth progress, and four 1.5 W LED lights to illuminate the ice from below. The combined heat input from LED lights and resistors was approximately 11.5 W. The heat input was chosen based on several trial runs investigating the sea ice crystal structure. It was high enough to prevent the formation of platelet ice crystals at the ice–water interface, i.e. supercooling of the water body was prevented. It was low enough to allow for the development of a lamellar interface with a skeletal layer thickness that appeared to be comparable the interface of naturally growing sea ice in winter and early spring (Petrich and Eicken, 2010). Approximately 0.1 m below the ice–air interface, crystals had a cross-sectional area of about 1 to 4 cm^2. It was found during trial runs with high ocean heat flux that ice lamellae were more difficult to discern visually, i.e., lamellae were supposedly flatter at the tips. The tank was placed in a temperature-controlled cold room that maintained continuous air circulation with temperature stability better than ±1 °C.

The tank was filled with Instant Ocean salt solution to 0.4 m depth. Two thermocouple probes were installed in the tank. Thermocouples protruded 20 mm horizontally from their respective support. One probe was installed at the side wall of the tank to measure temperature profile and growth rate of the ice cover in the "far field" of any oil lens. A second probe was installed at the center of the tank to determine ice growth and heat flux at the position of the oil lens (Figure 1a).

After water was cooled to approximately 0 °C, the ambient air temperature was set to -15 °C, initiating ice formation soon thereafter. This marks the start of the experimental run. Ice was grown to approximately 0.05 to 0.08 m thickness before a 0.15 x 0.15 m^2 insulator was placed at the center of the tank to locally retard ice growth and to form a depression in the ice–water interface. Similar methods are commonly used in field and laboratory experiments to produce oil lenses at specified locations (e.g., Nelson & Allan, 1982; Payne et al., 1991) as they simulate the insulating effect of the snow cover (e.g., Barnes et al., 1979; Petrich et al., 2012). This configuration placed the perimeter of the lens over 0.15 m from the side walls of the tank, eliminating the potential for encapsulation due to heat loss to the tank walls.

Four experiments were performed (#1, #3, #4, #5). Oil was injected under the ice either immediately after removal of the insulator (experiments #1 and #3), or approximately 12 hours after removal to allow the ice to adjust to the new atmospheric boundary condition before oil injection (experiments #4 and #5). At this time, ice thickness in the depression was approximately 0.07 to 0.1 m. Oil was injected under the depression through a hose deployed through a slot cut into the ice. Oil injection rate was approximately 50 μg/s. Individual oil drops impinged on the underside of the ice where they coalesced to form a single lens. Visual inspection showed that no air had been injected.

Ice growth was monitored automatically with temperature probes and under-tank cameras and by manual inspection through side windows of the tank. C-axis vertical platelets could be identified through the side windows due to total reflection when observed under shallow surface elevation angles. Ice thickness was determined from the position and freeze-in times of the thermocouples and manually by measuring ice thickness at the wall of the tank during temporary removal of the insulation. Since the ice–water interface is not necessarily planar at the walls, this manual method is not deemed to be particularly accurate. However, where

available, manually read off thickness compared well with ice thickness determined by the temperature probe at the wall.

At the end of the experiments, several vertical ice sections were excavated to determine vertical sea ice salinity profiles, crystal structure of ice both at the oil lens and at a distance, and geometry of the oil lens. Salinity was measured with a YSI 30 conductivity probe, giving salinity values on the dimensionless practical salinity scale (UNESCO, 1981). To obtain salinity data of small sample volumes, those sample volumes were diluted to increase volume, measured and scaled. Repeat calibration sets (triple sets) showed that the scaling is linear and that the random error of the salinity measurement is ±0.2. Due to the small size of samples, ice density and air volume has not been determined. However, air volume is expected to be negligible as experiments were finished before gasses dissolved in the water reached saturated concentration and air bubbles appeared under the ice.

RESULTS AND DISCUSSION

Ice Growth

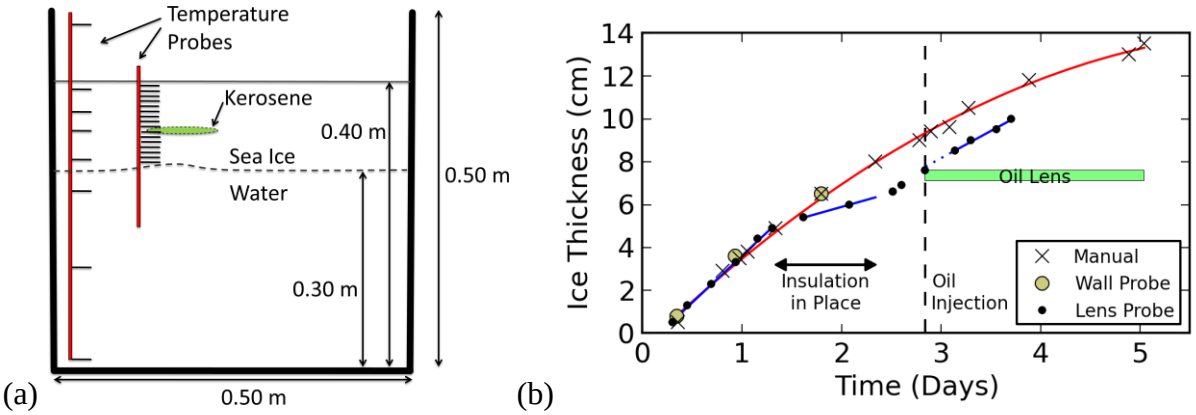

Figure 1. (a) Sketch of ice tank layout. (b) Ice growth data of oil injection experiment #5. Best fit are shown to guide the eye (blue: linear; red: second order polynomial).

Figure 1b shows ice thickness development for the example of experiment #5. For the first day of ice growth, ice thickness increased at approximately the same rate measured at the side wall of the tank (circles and crosses) and at the center (dots), i.e. at 5.0×10^{-7} ms^{-1}. Once insulation was in place, the ice growth rate beneath the insulation decreased noticeable to 1.5×10^{-7} ms^{-1}. However, growth rate increased again after removal of the insulation. After injection of oil, the ice growth rate under the oil lens was 2.9×10^{-7} ms^{-1}, comparable to the ice growth rate measured at the wall at this time of 2.7×10^{-7} ms^{-1}.

Atmospheric heat transfer during ice growth can be described by the turbulent atmospheric heat transfer coefficient. The heat transfer coefficient is defined as

$$h = \frac{k\dfrac{\Delta T_{ice}}{d}}{T_{air} - T_{surface}}, \qquad (1)$$

where k is the thermal conductivity of sea ice, d is the distance between the uppermost thermocouples at the wall that are in the ice, ΔT_{ice} is the temperature difference between these two thermocouples, T_{air} is the air temperature measured 0.06 m above the ice, and $T_{surface}$ is the ice surface temperature. The atmospheric heat transfer coefficient in the present series of experiments was constant throughout each experiment at 15 to 17 Wm^{-2}K^{-1}.

Ocean heat flux F_w was determined as the residual of latent heat flux ($\phi \rho L$ dH/dt >0) and heat conducted through the ice near the ice–ocean interface (k $\Delta T/\Delta z$ <0),

$$Fw + \phi\rho L \frac{dH}{dt} + k \frac{\Delta T}{\Delta z} = 0, \qquad (2)$$

where ρ and L are density and latent heat of fusion of freshwater ice, respectively, and ϕ and k are porosity and thermal conductivity of sea ice, respectively. In all experiments the ocean heat flux was determined to be F_w=±10 Wm^{-2}. Given the uncertainty in ϕ, k, and Δz, we cannot make any more definite statement beyond the notion that the ocean heat flux was small. This result is consistent with observations of crystal structure: the absence of distinct platelets growing into the water column indicated that the heat flux was not negative (i.e. there was no supercooling of the water body beyond constitutional supercooling). On the other hand, the presence of a zero-strength skeletal layer of approximately 0.02 to 0.05 m thickness indicated that the ocean heat flux was not particularly high.

Figure 2 shows an example of salinity, temperature, and porosity profiles at the end of experiment #4. Porosity was calculated with the equations of Cox & Weeks (1983). Salinity data are shown as measured in a profile through the oil lens and outside the lens area, between lens and wall. Salinity is high compared with field measurements of thick ice (e.g., Petrich & Eicken, 2010), presumably because desalination is still ongoing in this relatively thin ice. This is particularly likely considering that the porosity is consistently above 5% (Petrich & Eicken, 2010). The ice temperature profile is linear at the wall, above the lens, and under the lens. In addition, the respective temperature gradients are approximately equal, indicating that heat flow was predominantly one-dimensional. Profiles measured in other experiments were similar.

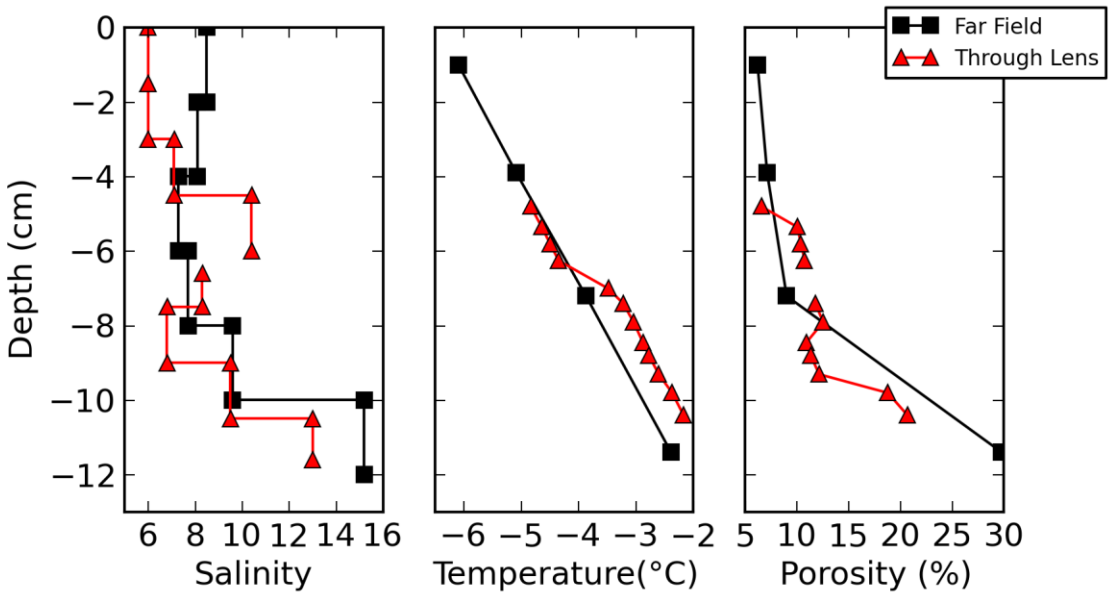

Figure 2. Sea ice salinity, temperature profile, and calculated porosity in experiment #4. Measurements are for the "far field" (squares), i.e. salinity and temperature measured between lens and wall and at the wall, respectively, and through the lens (triangles).

Temperature gradients measured at the wall, above and under the oil lens are summarized in Table 1 for experiments 3 to 5, i.e. all experiments with a temperature probe installed through the oil lens. Vertical temperature gradients in the ice were typically between 30 and 40 °C/m.

Uncertainty due to misalignment of thermocouples is estimated to be ±10%. Temperature gradients through the oil lens are approximately 4 times higher due to different thermal properties of the oil lens, discussed below. In order to calculate heat flux the thermal conductivity would need to be known, which depends on sea ice porosity and convection in the oil.

Encapsulation

The thickness of oil lenses were between 5 and 7 mm at the center of the lens, corresponding to the minimum lens thickness resulting from interfacial tension (NORCOR, 1975).

Temperature in the ice above the lens (<5 mm) changed rapidly during oil injection by up to 2 °C (based on temperature measurements taken once a minute), returning to its pre-injection value within 30 minutes. The temperature increased in all cases of warm oil injection but reduced temporarily after the injection of cold oil. This indicates that heat exchange took place between oil and ice.

Two ice growth modes contributed to encapsulation. On the one hand, ice around the lens formed a "lip" that provided additional resistance to lateral movement of the oil. It has been suggested that this phenomenon is due to distorted isotherms at the edge of the lens (Martin, 1979). Based on observations during the growth process (experiments #1, #3, #4), it appeared that the lamellae that formed the lip tended to grow tilted inward toward the lens (Figure 3). Apart from ice forming a lip, ice formed directly under the lens, starting with a layer of crystals with dominantly vertical c-axes. This layer grew to 5 to 10 mm thickness before it became overgrown by crystals with more horizontally aligned c-axes (Figure 4). This is in quantitative agreement with earlier studies (e.g., Payne et al., 1991). The thickness of these layers was determined after the end of the experiment from the alignment of the crystal fabric in vertical thick sections. Presence and extent of c-axis vertical crystals could be identified during growth based on total reflection at the ice–water interface when observed under shallow angles (Figure 5).

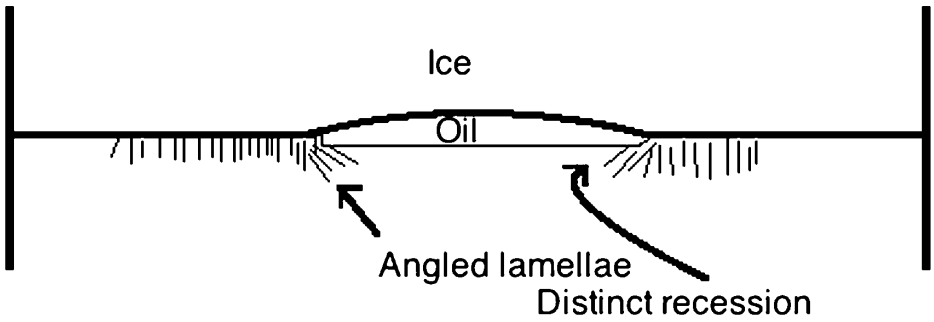

Figure 3. Concept sketch illustrating angled lamellae of the ice lip growing inward toward the lens. This configuration preceded overgrowth of the lens (experiments #1 to #4) except when the injected oil was cold (experiment #5).

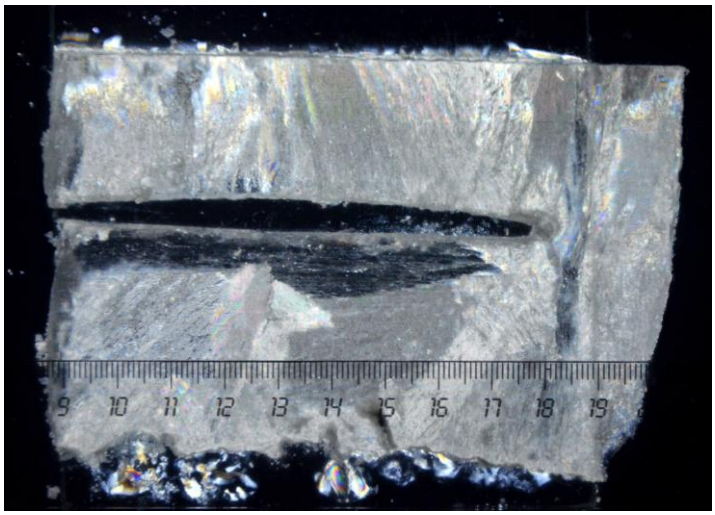

Figure 4. Vertical section under cross-polarized light (experiment #3). 5 to 10 mm of c-axis vertical crystals (dark) are visible under the oil lens (black). The ruler indicates distance in cm. Note that the ice was thicker than shown in this section.

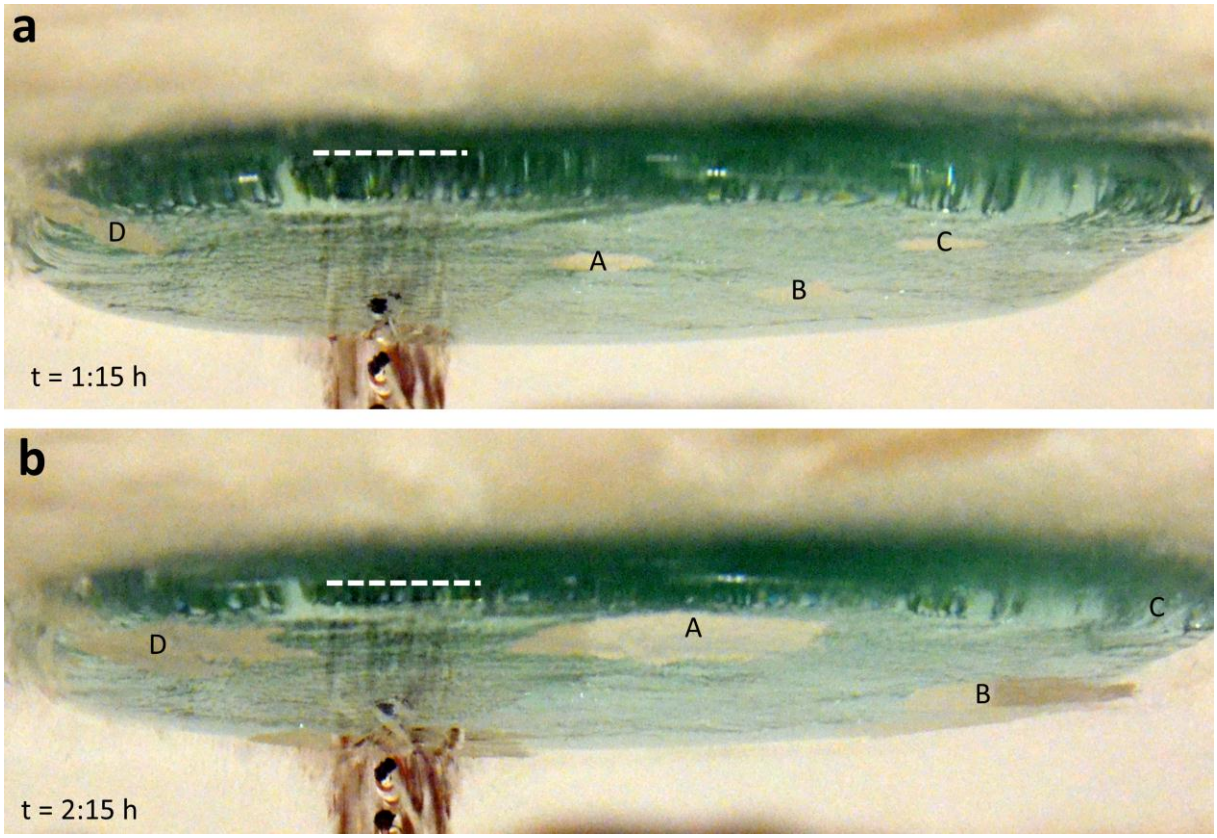

Figure 5. Oil lens (green) under sea ice (white) observed under shallow angle (a) 1:15 h and (b) 2:15 h after injection of cold oil in experiment #5. The width of the lens is approximately 10 cm. Markers A through D track growth and movement of individual crystals. The dashed line indicates the lower limit of the lip surrounding the lens. A temperature probe is located behind the lens with temperature sensor (black) protruding into the lens and water beneath (cf. Figure 1a). In (b), the sensor under the oil lens is partially covered by seemingly randomly aligned platelets, crystal B protrudes beyond the lens, and crystal C has slid off the lens.

We found evidence that both growth modes are in fact independent of each other. We found in experiments with warm oil that a lip extended beyond the thickness of the lens before the lens overgrew with c-axis vertical crystals. However, when cold oil had been injected (experiment #5), we observed 1:15 h after injection a partial cover with c-axis vertical crystals while the lip extending to estimated 40% of the lens thickness (Figure 5a). The lip reached the thickness of the lens not until 2 h after injection. To our knowledge, the only previous report of overgrowth without a lip surrounding the lens first has been given by Wolfe & Hoult (1974) who flooded the entire underside of their laboratory-grown ice with oil, removing any possibility for lip formation.

The timing of the initial formation of c-axis vertical crystals was found to depend significantly on ice and oil temperature. With warm oil (T>-1.9 °C) injected immediately after the removal of the surface insulation, i.e. while the ice above the depression was warm, formation of these crystals started between 4.5 to 5.5 hours after injection (experiments #1 and #3). With warm oil injected while ice above the depression was in quasi-steady state, formation of these crystals started between 1.5 to 2.5 hours (experiment #4). With cold oil (T<-1.9 °C) injected while ice above the depression was in quasi-steady state, formation of these crystals started within 1 hour of oil injection (most likely within less than 30 minutes) (experiment #5). In the latter case, individual crystals nucleated at several locations across the oil–water interface. They were mobile, sliding across the oil–water interface while increasing in size (Figure 5). Evidence was found of crystals sliding off the lens (crystal C in Figure 5b). Such crystals likely provide a basis for lens overgrowth with crystals of non-vertical c-axes.

Heat Transfer

While heat transfer through the ice is by conduction, heat transfer through the oil lens may be either by conduction or by convection (e.g., Wolfe & Hoult, 1974). In the case of predominantly one-dimensional heat transfer through the lens,

$$\left(k\frac{dT}{dz}\right)_{ice\ above oil} = \left(k\frac{dT}{dz}\right)_{oil} = \left(k\frac{dT}{dz}\right)_{ice\ below oil}, \qquad (3)$$

i.e.

$$\frac{(dT/dz)_{oil}}{(dT/dz)_{ice}} = \frac{k_{ice}}{k_{oil}}. \qquad (4)$$

Our estimates of temperature gradient measurements through the oil lens are slightly underestimated since at least one thermocouple was actually embedded in the ice in each experiment. However, Table 1 indicates that the temperature gradient through the oil was around 4 times higher than the gradient through ice. On the other hand, the thermal conductivity of sea ice (k_{ice}=1.8 $Wm^{-2}K^{-1}$) is over 11 times higher than the thermal conductivity of kerosene (k_{oil}=0.16 $Wm^{-2}K^{-1}$ below 0 °C). This difference results from convective heat transport though the oil. Convective heat transport due to natural convection is expected to occur once the Rayleigh number, Ra, exceeds a critical value, Ra_c, which depends on the boundary conditions of the domain. For infinite plane-parallel surfaces with rigid boundaries of constant and homogeneous temperature, Ra_c=1708. With

$$Ra = \frac{g \frac{\partial \rho}{\partial T} \Delta T \, L^3}{\mu \alpha}, \qquad (5)$$

and g=9.81 ms^{-2}, lens thickness L=0.007 m, temperature difference between upper and lower interface of the lens ΔT=0.8 °C (cf. Table 1, experiment #5), thermal expansion of kerosene dρ/dT=0.8 kgm^{-3}K^{-1}, thermal diffusivity and dynamic viscosity of kerosene α=10^{-7} m^{2}s^{-1} and μ=2.5 mPa s, respectively, we find that Ra=8600, i.e. convective heat transport should have taken place in all experiments.

SUMMARY AND CONCLUSION

Encapsulation experiments of oil under sea ice were performed. Observations were consistent with previous reports and include both lip formation around the oil lens and overgrowth of the lens by initially c-axis vertical crystals. In addition to previous reports, we found that overgrowth with c-axis vertical crystals can be initiated much faster than previously reported. In particular, in one experiment using cold oil, overgrowth was initiated less than one hour after injection and clearly preceding ice lip formation around the lens. This indicates that ice formation around and under a lens should be treatable as a heat flow problem with phase transition, similar to earlier numerical simulations of ice growth (e.g., Petrich et al., 2006). In particular, there is no evidence in present and past experiments (e.g., Wolfe & Hoult, 1974) that crystal alignment and the presence of a lip prior to overgrowth will need to be accounted for explicitly.

Heat transfer through the oil lens was by convection in the present experiments, consistent with common scaling relationships.

Based on the presented measurements and previous reports we conclude that the process of separation of oil lenses form the ocean by encapsulation appears to be governed by common thermodynamic and fluid dynamic principles and should therefore be tractable in a relatively straight-forward manner.

Table 1. Temperature gradients determined above, through and below the oil lens and near the ice–air surface. Ice thickness was measured at the wall rather than under the lens. No probe through was installed through the lens in experiment #1.

Temperature gradient (°C/m)	**Experiment #3**	**Experiment #4**	**Experiment #5**
Near Ice Surface Above Lens	not measured	not measured	43
Above Lens	32	33	35
Through Lens	155	115	112
Below Lens	38	39	39
Wall	40	36	42
Ice Thickness	13.5 cm	13.0 cm	12.5 cm

ACKNOWLEDGEMENTS
This work was funded through The Research Council of Norway project number 195160 (Northern Environmental Waste Management) and Eni Norge. Data acquisition and analysis was supported by The Research Council of Norway project number 195153 (ColdTech).

REFERENCES

Barnes, P. W., Reimnitz, E., Toimil, L., and Hill, H., 1979. Fast ice thickness and snow depth relationships related to oil entrapment potential, Prudhoe Bay, Alaska. In Proceedings of the 5th International Conference on Port and Ocean Engineering Under Arctic Conditions (POAC), Norwegian Institute of Technology, Trondheim, Norway, 13–18 Aug 1979, 1205–1225.

Cox, G. F. N., and Weeks, W. F., 1983. Equations for determining the gas and brine volumes in sea-ice samples. Journal of Glaciology, 29(102), 306–316.

Dickins, D. F., 2011. Behavior of Oil Spills in Ice and Implications for Arctic Spill Response. In: Proceedings of the OTC Arctic Technology Conference, 7-9 February 2011, Houston, Texas, USA, OTC 22126, 1–15.

Dickins, D. F., 1992. Behavior of Spilled Oil at Sea (BOSS): Oil-in-Ice Fate and Behavior, Environment Canada, U.S. Minerals Management Service, and American Petroleum Institute. 342 pp.

Karlsson, J., Petrich, C., and Eicken, H., 2011. Oil entrainment and migration in laboratory-grown saltwater ice. In Proceedings of the 21st International Conference on Port and Ocean Engineering under Arctic Conditions (POAC), Montreal, Quebec, Canada, 10–14 July 2011. Paper POAC11-186, 10 pp.

Martin, S., 1979. A field study of brine drainage and oil entrainment in first-year sea ice, Journal of Glaciology, 22(88), 473–502.

Nelson, W. G. and Allen, A. A., 1982. The Physical Interaction and Cleanup of Crude Oil with Slush and Solid First Year Ice. Proceedings of the Fifth Arctic Marine Oil Spill Program Technical Seminar, 1982, 37-59.

NORCOR Engineering and Research Ltd., 1975. The interaction of crude oil with Arctic sea ice. Beaufort Sea Technical Report No. 27. Beaufort Sea Project, Department of the Environment, Victoria, BC, Canada. 201 pp.

Payne, J. R., McNabb Jr., G. D., and Clayton Jr., J. R., 1991. Oil-weathering behavior in Arctic environments, Polar Research 10(2), 631–662.

Petrich, C., and Eicken, H., 2010. Growth, Structure and Properties of Sea Ice. In Thomas and Dieckmann (eds), Sea Ice, 2nd ed, Wiley–Blackwell, pp. 23–77.

Petrich, C., Eicken, H., Polashenski, C. M., Sturm, M., Harbeck, J. P., Perovich, D. K., and Finnegan, D. C., 2012. Snow dunes: a controlling factor of melt pond distribution on Arctic sea ice. Journal of Geophysical Research, 117, C09029, 1–10, http://dx.doi.org/10.1029/2012JC008192.

Petrich, C., Karlsson, J., and H. Eicken, H., 2013. Porosity of growing sea ice and potential for oil entrainment. Cold Regions Science and Technology, 87, 27–32, http://dx.doi.org/10.1016/j.coldregions.2012.12.002.

Petrich, C., Langhorne, P. J., and Sun, Z. F., 2006. Modelling the interrelationships between permeability, effective porosity and total porosity in sea ice, Cold Regions Science and Technology, 44(2), 131–144, http://dx.doi.org/10.1016/j.coldregions.2005.10.001.

UNESCO, 1981. Tenth report of the joint panel on oceanographic tables. Unesco technical papers in marine science, 36, 25 pp.

Wolfe, L. S., and Hoult, D. P., 1974. Effects of oil under sea ice, Journal of Glaciology, 13(69), 473–488.